INTERNATIONAL JOURNAL FOR NUMERICAL METHODS IN FLUIDS, VOL. 21, 155–180 (1995)

DECAY OF CONFINED, TWO-DIMENSIONAL, SPATIALLY PERIODIC ARRAYS OF VORTICES: A NUMERICAL INVESTIGATION

DANIEL T. VALENTINE

Department of Mechanical and Aeronautical Engineering, Clarkson University, Potsdam, NY 13699-5725, U.S.A.

SUMMARY

The disarrangement of a perturbed lattice of vortices was studied numerically. The basic state is an exponentially decaying, exact solution of the Navier–Stokes equations. Square arrays of vortices with even numbers of vortex cells along each side were perturbed and their evolution was investigated. Whether the energy in the perturbation grows somewhat before it decays or decays monotonically depends on the initial strength of the vortices of the basic state, the extent of lateral confinement and the structure of the perturbation. The critical condition for temporally local instability, i.e. the critical amplitude of the basic state that must be exceeded to allow energy transfer from the basic state to the perturbation, is discussed. In the strongly confined case of a square lattice of four vortices the appearance of enchancement of global rotation is the result of energy transfer from the basic state to a temporally local unstable mode. Energy is transferred from the basic state to larger-scaled structures (inverse cascade) only if the scales of the larger structures are inherently contained in the initial structure of the perturbation. The initial structure of the double array of vortices is *not* maintained except for a very special form of perturbation. The facts that large scales decay more slowly than small scales and that, when non-linearities are sufficiently strong, energy is transferred from one scale to another explain the differences in the disarrangement process for different initial strengths of the vortices of the basic state. The stronger vortices, i.e. the vortices perturbed in a manner that increases their strength, tend to dominate the weaker vortices. The pairing and subsequent merging (or capture) of vortices of like sense into larger-scale vortices are described in terms of peaks in the evolution of the square root of the palinstrophy divided by the enstrophy.

KEY WORDS: computational fluid dynamics; finite-difference method; Navier–Stokes equations

1. INTRODUCTION

Over the last several years there has been growing interest in vortical flows that are predominantly two-dimensional. It is evident that they are not only of pedagogical interest but also of practical interest. Predominantly two-dimensional motions with vortical structures occur, for example, in the atmospheres of several of the planets in our solar system in the form of large-scale motions. Two-dimensional vortical structures have also been observed in experiments in rotating tanks, in stratified fluids and in electromagnetically driven flows in liquid metals. The interactions of vortical structures play an important role in turbulent flows. Numerical simulations of 'two-dimensional turbulence' illustrate the dominance of two-dimensional vortex interactions and vortex captures (merging of vortices of like sense) in sustaining and dissipating turbulent kinetic energy. Investigations of two-dimensional, spatially periodic flows have helped in interpreting experimental observations in liquid metal flows. The disarrangement of decaying vortex lattice flows when subject to a small perturbation

CCC 0271–2091/95/020155–26

Received 25 November 1992
Revised 27 December 1994

described herein has identifiable features similar to those found in decaying two-dimensional 'turbulence' and in linearly perturbed driven vortex lattice flows.

A direct simulation of the decay process of two-dimensional Navier–Stokes turbulence was investigated by McWilliams[1] and more recently by Matthaeus *et al.*[2] Matthaeus *et al.* computed the evolution of a decaying flow field over a much longer interval of time than originally studied by McWilliams. Their computations showed that as time progresses, 'all possible like-sign vortex captures occur, leaving us with one vortex of either sign. The final-state stream function contours bear a striking resemblance to those for a basic cell of an Ewald lattice'. Alternatively, within the context of the figures they presented, the final state resembles the basic structure of a pair of cells of the exact solution of the Navier–Stokes equations published by Taylor,[3] which represents an infinite array of counter-rotating vortices. Motivated by interests in examining the transfer of energy between scales in two-dimensional 'turbulence', the stability of two-dimensional cellular flows has been investigated by Green,[4] Gotoh *et al.*,[5] Gotoh and Yamada[6] and Beaumont.[7] The inverse cascade in two-dimensional turbulence has also been pondered by, among others, Frish and Sulem.[8]

The possibility of generating predominantly two-dimensional periodic flows using an electromagnetic effect has been amply demonstrated in the literature. The papers by Thess,[9,10] Sommeria,[11] Sommeria and Verron[12] and Verron and Sommeria[13] are on spatially periodic driven (forced) flows. They examined the creation and stability of Kolmogorov flows and flows of square arrays of vortices. The chaotic behaviour of Kolmogorov flows, under appropriate conditions, has been examined by Platt *et al.*[14] Various flow regimes were identified depending on the Reynolds number; they observed periodic, chaotic and relaminarization windows in each flow regime. Thess[10] presented the critical condition for linear instability that must be exceeded for the 'first' unstable mode to be excited in a perturbed, forced, square lattice of vortices. Thess also examined the effects of lateral confinement on the stability of this class of flows.

The decaying vortex lattice in an infinite domain is an exact solution of the Navier–Stokes equations that was originally published by Taylor.[3] It is a double array of two-dimensional vortices in a domain of infinite extent. The vortices decay exponentially with time. This solution is one of a class of flows that Eringen[15] has called Taylor flows. Whitham, in an article in the book edited by Rosenhead,[16] cited this solution and Kovasznay's[17] solution when he discussed exact non-parallel flow solutions of the Navier–Stokes equations. The solution originally published by Kovaznay is a model of an infinite cascade of steady, two-dimensional wakes. Both solutions have been examined recently by Lin and Tobak[18,19] and Chen[20] from the viewpoint of stability theory. A characteristic feature of Taylor flows is that the two non-linear terms of the Navier–Stokes equations, although individually relatively large, cancel.

The present investigation is a numerical study of the effect of perturbing the two-dimensional array of counter-rotating vortices reported by Taylor.[3] Numerical computations were made to investigate the disarrangement caused by perturbations of confined lattices of vortices that are decaying with time from an initial state corresponding to a perturbed Taylor array. The numerical solutions were obtained by solving the Navier–Stokes and continuity equations in terms of vorticity and streamfunction variables. The system of non-linear equations was solved by applying two methods. The first method is a fourth-order implicit method developed by Mohamed *et al.*,[21] the computer code that implements this method is still under development. The second method is a two-step, explicit-in-time, upwind finite difference method; it is the first-order-in-time, second-order-in-space ETUDE scheme developed by Valentine.[22,23] The latter method is relatively efficient and requires less computer time to execute. Hence most of the results presented were computed by the second method. The results of the numerical simulations are compared with the theoretical results of stability of the Taylor array reported by Lin and Tobak[18,19] and Chen.[20] The discussion also takes advantage of the results reported by Thess[10] for the driven lattice.

The present results demonstrate *a fortiori* the fact that large-scale eddies decay significantly more slowly than small-scale eddies. In addition, the predictions show the influence of the size of the domain (or the lateral confinement of the vortex lattice), the modal structure of the initial condition and the strength of the vortices at the start of the motion on the ensuing flow patterns. It was found that the long-time structure of the decaying flow field depends on the modal structure, i.e. the spatial scales, of the perturbation as well as of the basic state. For a sufficiently strong initial condition of the basic flow field, if it is perturbed, the pairing and merging of vortices of like sign occur. Vortex mergings and captures occur until the largest scales inherently present in the initial condition finally decay. Also, since the largest scales decay much more slowly than the smaller scales, they tend to dominate the long-time solution. The evolution of this non-linear process is discussed in terms of the interaction of Fourier modes as determined by applying a two-dimensional FFT at each time step in the computation. Merging involves the transfer of energy from the basic state to the perturbation, which is easily visualized by an examination of the Fourier modes of the system and the evolution of the square root of the palinstrophy divided by the enstrophy. In addition, the structure of the 'most unstable mode' is identified and found to compare favourably with the same predicted by linear stability theory. The most unstable mode is defined here as the primary mode that draws energy from the basic state, thus accelerating the decay of the basic state. This is a good example of subharmonic interaction.

An outline of this paper is as follows. In the next section the methodology applied to obtain and evaluate the computational results is outlined. The outline includes a description of the model equations, stability considerations, integral quantities that are useful in describing the merging of vortices and the computational methods applied to solve the model equations. The subsequent section presents the results and provides a discussion. The results and discussion are subdivided into low-Reynolds-number cases that may be described as a superposition of Taylor (or Stokes) modes and moderate-Reynolds-number cases that illustrate both linear and non-linear modal interactions. The last section is a summary of conclusions.

2. METHODOLOGY

2.1. Model equations

The model equations for the two-dimensional flow of an incompressible Newtonian fluid are the Navier–Stokes (NS) and continuity equations. In terms of the vorticity ω and streamfunction ψ the model equations are

$$\frac{\partial \omega}{\partial t} + \frac{\partial \psi}{\partial z}\frac{\partial \omega}{\partial x} - \frac{\partial \psi}{\partial x}\frac{\partial \omega}{\partial z} = \frac{\partial^2 \omega}{\partial x^2} + \frac{\partial^2 \omega}{\partial z^2}, \tag{1}$$

$$\omega = \frac{\partial^2 \psi}{\partial x^2} + \frac{\partial^2 \psi}{\partial z^2}. \tag{2}$$

Equations (1) and (2) are in the non-dimensional form. The characteristic velocity was taken to be $U = \nu/d$, where d is the characteristic dimension or size of one of the vortex cells of the Taylor double array (which will be described next). The Reynolds number $Re = Ud/\nu = 1$; therefore it does not appear in the above equations.

The flow field examined in this investigation is an exact solution of equations (1) and (2). It was published by Taylor.[3] He recognized that if $\omega = f(\psi)$, the non-linear terms in equation (1) cancel (this is the peculiar characteristic of all Taylor flows). The special case considered by Taylor is $\omega = -k\psi$, where k is an arbitrary constant. The solution he published may be written as

$$\psi = \mathscr{R} \sin(nx)\sin(mz)e^{-(n^2+m^2)t}, \tag{3}$$

where $\mathscr{R}$ is an arbitrary constant. The velocity field $\mathbf{u} = (u, w)$ is given in terms of the stream-function ψ by the relationships

$$u = \frac{\partial \psi}{\partial z}, \qquad w = -\frac{\partial \psi}{\partial x}.$$

Thus the corresponding velocity field for this flow is

$$\mathbf{u} = \mathscr{R} e^{-(n^2+m^2)t}[m \sin(nx)\cos(mz)\mathbf{i} - n \cos(nx)\sin(mz)\mathbf{k}].$$

$\mathscr{R}$ is a measure of the highest velocity in the flow field at $t = 0$. It is scaled by U. Thus $\mathscr{R}$ is a Reynolds number that describes the strength of the initial condition, i.e. the Reynolds number $R \equiv (\mathscr{R}U)d/\nu = \mathscr{R}$. This flow field is a double array of vortices that decay exponentially in time. This solution is for the infinite domain $-\infty < x < \infty$, $-\infty < z < \infty$. Also, the time varies in the range $0 < t < \infty$. Figure 1 illustrates 16 cells of the infinity of cells in Taylor's $n = m$ periodic array.

The computational problem examined in the present investigation is an extension of the Taylor problem for which the solution is computed in a square subdomain along the boundaries of which the exact solution is specified, i.e. it is a square lattice in the confined domain $0 \leq x \leq \pi$, $0 \leq z \leq \pi$. The boundary value problem for a 4×4 or 16-cell vortex array satisfies equations (1) and (2) in the domain $0 < x < \pi$, $0 < z < \pi$ for $n = m = 4$; this case is illustrated in Figure 1. The boundary conditions for this problem are

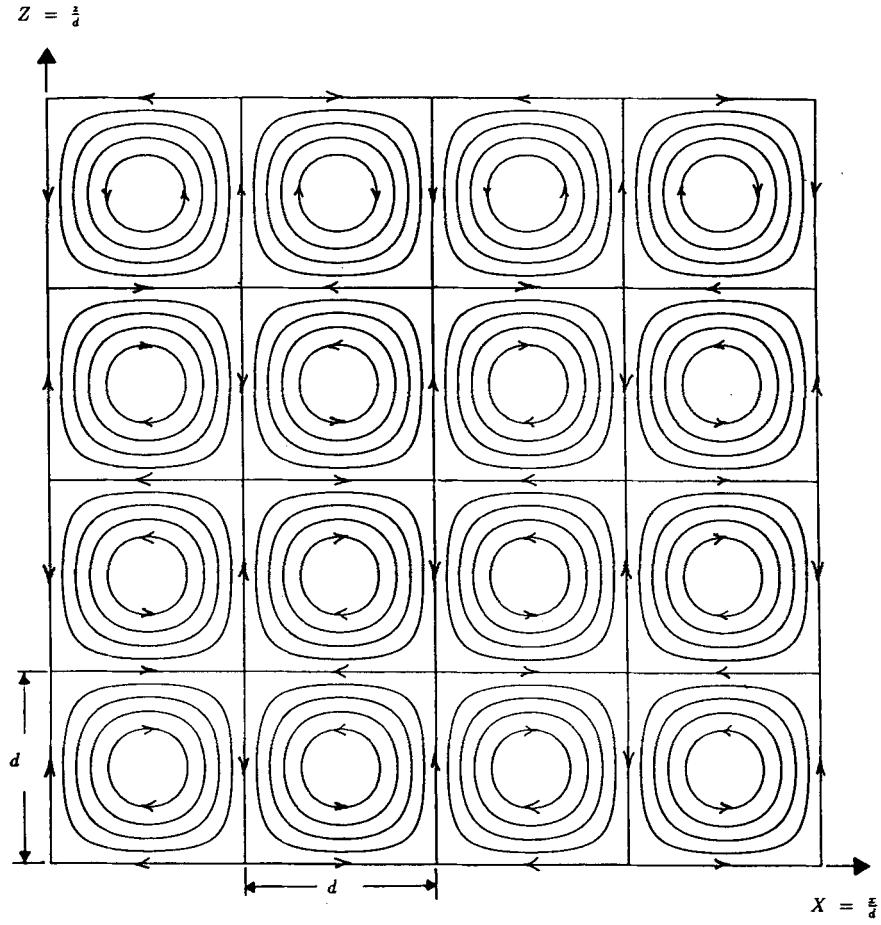

Figure 1. Illustration of Taylor's double array of vortices; $-1 \leq \psi \leq 1$, $\Delta\psi = 0{\cdot}2$

(a) $\psi = 0$, $\omega = 0$ for $0 < x < \pi$, $z = 0$
(b) $\psi = 0$, $\omega = 0$ for $x = 0$, $0 < z < \pi$
(c) $\psi = 0$, $\omega = 0$ for $0 < x < \pi$, $z = \pi$
(d) $\psi = 0$, $\omega = 0$ for $x = \pi$, $0 < z < \pi$

Note that $\omega = -(n^2 + m^2)\psi$ for the basic state. This flow field was perturbed and its evolution was studied in regions that were laterally confined, i.e. in square regions where $0 \leq x \leq \pi$, $0 \leq z \leq \pi$ for basic states such that $n = m$ and $n = 2, 4, 6, \ldots$ (square lattices with even numbers of cells along each side). The initial condition for ω that was imposed at the onset of the computations was found by substituting equation (3) into the expression for ω and adding the perturbation to ω. The perturbation is *zero* at the boundaries for all times t; hence the domain is confined laterally. The initial condition for ψ is subsequently determined by solving equation (2). The transient solution for $t > 0$ is sought. $\mathscr{R} = 1$, 100 and -50 were among the initial strengths of the basic state considered in this study. A precise description of the initial conditions imposed will be presented with the results, because it is the different types of perturbations that distinguish the different cases.

2.2. *'Stability' considerations*

In this subsection the linear stability theory that may be applied to help describe the persistence of the flow pattern of the basic state of a confined, decaying lattice of vortices subject to an infinitesimal perturbation at time $t = 0$ is described. The assumptions required to simplify the theory to take advantage of the results presented by Thess[10] for the driven vortex lattice are outlined. The reason for presenting the following analysis of the stability of the decaying array is because the most persistent mode that characterizes the perturbation in the present study has the same modal structure as the most (or 'first') unstable (linear) mode that Thess found for the driven lattice.

It is known that the basic state with or without perturbation is globally stable. This is not surprising, because for $t > 0$ no additional energy is added to the system. However, the question of stability raised here is whether or not the structure of the perturbation imposed can drain energy from the basic state with concomitant (temporary) growth of its scale (albeit the total energy of the system unquestionably decays as time progresses). To address this question, an approximate equation governing the initial stages of growth of infinitesimal perturbations, i.e. the linearized equation that governs the dynamics of the perturbation assuming the basic state is known and persists, is derived next.

If we substitute equation (2) into equation (1) and let $X = 2Nx$ and $Z = 2Nz$ (to aid in the comparison with the work of Thess[10]), we get the following equation for ψ:

$$\frac{\partial(\nabla^2\psi)}{\partial\tau} + \frac{\partial\psi}{\partial Z}\frac{\partial(\nabla^2\psi)}{\partial X} - \frac{\partial\psi}{\partial X}\frac{\partial(\nabla^2\psi)}{\partial Z} = \frac{\partial^2(\nabla^2\psi)}{\partial X^2} + \frac{\partial^2(\nabla^2\psi)}{\partial Z^2}, \tag{4}$$

where

$$\nabla^2\psi \equiv \frac{\partial^2\psi}{\partial X^2} + \frac{\partial^2\psi}{\partial Z^2}.$$

From this equation we can derive an equation that models the evolution of an infinitesimal perturbation. This is done next. Let

$$\psi = \psi_0 + \psi_1, \tag{5}$$

where

$$\psi_0 = \mathscr{R}e^{-2\tau}\sin(X)\sin(Z).$$

Substituting this decomposition of the streamfunction into equation (4) and dropping the non-linear terms in ψ_1 (assuming ψ_1 is infinitesimally small), we obtain

$$\frac{\partial\nabla^2\psi_1}{\partial\tau} = \nabla^2(\nabla^2\psi_1) + \mathscr{R}e^{-2\tau}\cos(X)\sin(Z)(\nabla^2 + 2)\frac{\partial\psi_1}{\partial Z} - \mathscr{R}e^{-2\tau}\sin(X)\cos(Z)(\nabla^2 + 2)\frac{\partial\psi_1}{\partial X}. \tag{6}$$

The next step is to expand ψ_1 in a Fourier sine series. Let

$$\psi_1 = \sum_{n,m=1}^{\infty} \phi_{nm} \sin\left(\frac{nX}{2N}\right)\sin\left(\frac{mZ}{2N}\right), \tag{7}$$

where $\phi_{nm} = \phi_{nm}(t)$ and

$$0 \leq X \leq 2\pi N, \qquad 0 \leq Z \leq 2\pi N.$$

Substituting this expansion into equation (6), projecting the solution by multiplying each term by $\sin(pX/2N)\sin(qX/2N)$ and applying the orthogonality conditions of the eigenfunctions to extract the (nm)th term, and truncating the re-expanded terms at M, we get the following system of ordinary differential equations for the unknown Fourier coefficients:

$$\begin{aligned}\frac{\mathrm{d}\phi_{nm}}{\mathrm{d}t} = &-\left(\frac{n^2}{4N^2}+\frac{m^2}{4N^2}\right)\phi_{nm} + \frac{1}{8N}\sum_{p,q=1}^{M}\phi_{pq}\mathscr{R}\mathrm{e}^{-2\tau}\frac{2-(p^2/4N^2+q^2/4N^2)}{n^2/4N^2+m^2/4N^2}\\ &\times[p(\delta_{p,n-2N}-\delta_{p,n+2N}+\delta_{p,-n+2N})(\delta_{q,m-2N}+\delta_{q,m+2N}-\delta_{q,-m+2N})\\ &-q(\delta_{p,n-2N}+\delta_{p,n+2N}-\delta_{p,-n+2N})(\delta_{q,m-2N}-\delta_{q,m+2N}+\delta_{q,-m+2N})].\end{aligned} \tag{8}$$

This equation can only be true near $\tau = 0^+$. This is because if the basic state is unstable, its energy will be transferred to the perturbation, with the consequence that its rate of decay will be accelerated. Let us assume that $\mathscr{R}\mathrm{e}^{-2\tau} \approx \mathscr{R}$ near $\tau = 0^+$ (this assumes that the magnitude of the growth rate is significantly larger than the magnitude of the decay rate of the basic state). Let us next assume that we may write $\phi_{nm}(t) = C_{nm}e^{\lambda t}$. With these assumptions we *over*simplify equation (8) to get the algebraic eigenvalue problem

$$\begin{aligned}\Lambda C_{nm} = &-\Upsilon\left(\frac{n^2}{4N^2}+\frac{m^2}{4N^2}\right)C_{nm} + \frac{1}{8N}\sum_{p,q=1}^{M}C_{pq}\frac{2-(p^2/4N^2+q^2/4N^2)}{n^2/4N^2+m^2/4N^2}\\ &\times[p(\delta_{p,n-2N}-\delta_{p,n+2N}+\delta_{p,-n+2N})(\delta_{q,m-2N}+\delta_{q,m+2N}-\delta_{q,-m+2N})\\ &-q(\delta_{p,n-2N}+\delta_{p,n+2N}-\delta_{p,-n+2N})(\delta_{q,m-2N}-\delta_{q,m+2N}+\delta_{q,-m+2N})],\end{aligned} \tag{9}$$

where $\Upsilon = 1/\mathscr{R}$ and $\Lambda = \lambda/\mathscr{R}$. The parameter Λ is a set of complex eigenvalues $\Lambda_l = \Lambda_{lr} + i\Lambda_{li}$, $l = 1, 2 \ldots$. This equation is identical with equation (10) in Thess's[10] paper; of course, the interpretation of Λ and Υ are different.

Equation (9) was *not* solved in this investigation; it was solved by Thess.[10] The solutions he reported are instead reinterpreted and utilized to help examine the numerical results reported in this paper. He reported solutions for driven square lattices corresponding to $N = 1$ (2×2 cells), $N = 2$ (4×4 cells) and $N = \infty$ (infinity of cells). His work included linear Hartmen friction as well as viscous friction in the equations of motion. The zero-Hartmen-friction solutions are the only ones of interest in the present study. The critical values for $N = 1$ (or $n = m = 2$), $N = 2$ (or $n = m = 4$) and $N = \infty$ are $\Upsilon_c = 0{\cdot}2371$ (or $\mathscr{R}_c = 4{\cdot}22$), $\Upsilon_c = 0{\cdot}3198$ (or $\mathscr{R}_c = 3{\cdot}13$) and $\Upsilon_c = 0{\cdot}3536$ (or $\mathscr{R}_c = 2{\cdot}83$) respectively. The first two cases are vortex lattices that are confined laterally by pure slip rigid walls. The third case is an infinite lattice of vortices. The effect of restricting the motion of the walls of the system is to make it more stable, i.e. the critical Reynolds number is higher for the laterally confined cases. The temporary growth or *alteration of the decay rate* of an 'unstable' mode occurs when $\mathscr{R} > \mathscr{R}_c$. This growth at some instant of time may be called a temporally local instability. In addition, the structure of the 'first unstable mode' reported by Thess for the 2×2 forced square lattice is identical with the most persistent ('unstable') mode predicted in the present study for the decaying 2×2 square lattice.

2.3. *Integrals of vortex merging*

At each time step in the numerical simulation a double Fourier sine series decomposition was performed to determine the modal composition of the vortical flow field as it evolved. The Fourier decomposition not only provided information about the temporal variation in the structure of the perturbation as well as the basic state, but also provided a convenient method for computing the total kinetic energy, enstrophy and palinstrophy at each time step. These parameters are defined next. The Fourier decomposition of the vorticity is

$$\omega = \sum_k \hat{\omega}(k,\ t)\sin(n\pi x)\sin(m\pi z),$$

where $k^2 = n^2 + m^2$. The total kinetic energy per unit mass may be written in terms of the vorticity as

$$E \equiv \sum_k E(k) = \sum_k \tfrac{1}{2}|\hat{\mathbf{u}}(k)|^2 = \sum_k \frac{1}{k^2}|\hat{\omega}(k)|^2.$$

The enstrophy is the mean squared vorticity, i.e.

$$\Omega \equiv \langle \tfrac{1}{2}\omega^2 \rangle = \tfrac{1}{2}\sum_k |\hat{\omega}(k)|^2.$$

The angle brackets in this equation imply the mean spatial average. The palinstrophy is a parameter that governs the enstrophy dissipation rate and is defined as

$$P \equiv \tfrac{1}{2}\sum_k k^2|\hat{\omega}(k)|^2.$$

According to Matthaeus *et al.*,[2] the computed square root of the ratio of enstrophy to energy, i.e. $\sqrt{(\Omega/E)}$, decays monotonically with time for the types of decaying flow fields studied in their and in the present study. Matthaeus *et al.* reported that this fact is supported on theoretical grounds. The computational experiments they reported as well as the numerical simulations reported herein support this fact. This fact illustrates that enstrophy decays faster than energy.

On the other hand, the manifestation of peaks (or 'sharp spikes') in the variation of the square root of the ratio of palinstrophy to enstrophy, i.e. $\sqrt{(P/\Omega)}$, with time identifies the merger (or capture) events of vortices. The mergers of vortices in the present study are of the type characterized by peaks in the $\sqrt{(P/\Omega)}$ curve in the same way the capture events were characterized by Matthaeus *et al.*[2] in their numerical simulation of decaying two-dimensional 'turbulence'. The long-time behaviour of their solution is manifested in a lattice of vortices of a single size (the 'Ewald' lattice). These vortices are most likely the largest scales of the motion imposed at the initial state of the problem. This conclusion is based on the results of the present numerical simulations and the long-time streamline pattern of the flow field reported by Matthaeus *et al.*

2.4. *Computational methods*

Equations (1) and (2) were solved numerically by applying two computational methods. The first method was developed by Mohamed *et al.*[21] and is summarized next.

The system of coupled, time-dependent, non-linear partial differential equations was solved by applying a variable time step Crank–Nicolson scheme with Richardson extrapolation to approximate the timewise integration. The elliptic problems at the core of the method were solved by a fourth-order collocation method. The non-linearities were solved by an iteration procedure from one time step to the

next. This iteration procedure is repeated until the computed values of ω and ψ converge to within the prescribed error tolerance. This iterative procedure is similar to Gauss–Siedel iteration for a set of linear algebraic equations. As in the linear algebra analogue, the iteration may or may not converge and the convergence is directly affected by how the equations and unknowns are ordered. Since the time steps δt are selected by an algorithm that controls the error of the transient solution and since the error bound selected is relatively small, convergence problems have *not* been experienced. This procedure was set up so that a single linear elliptic problem is solved at each step; hence we could apply one of the subprogrammes in ELLPACK to solve the linear elliptic problems. The software tools available in ELLPACK are fully described by Rice and Boisvert.[24] The elliptic equations are solved by applying the fourth-order collocation method in ELLPACK. The method is a finite element method that uses Hermite bicubic piecewise polynomial approximations. The coefficients of the approximations are determined to satisfy the elliptic problem exactly at a set of collocation points. Similarly, the boundary conditions are satisfied exactly at a set of collocation points on the boundary. The resulting banded matrices are solved by applying the LINPACK band solver described by Dongarra *et al.*[25] The scheme is fourth-order in time and fourth-order in space. The desired accuracy, as required by the user, is specified by appropriate selections of the grid size, the time step and the error bounds imposed on the iteration procedures.

To verify the fourth-order code, a numerical simulation of four cells of the unperturbed non-parallel flow solution of Taylor[3] with $\mathscr{R} = 1$ was computed. The non-linear terms in equation (1) for Taylor's solution are individually about the same size as the other terms in this equation. The computer code computes these terms; the sum of these terms is supposed to be equal to zero. The computational method being tested must verify this fact. The results of this simulation with the fourth-order code were reported by Valentine and Mohamed.[26,27] The grid size selected by Valentine and Mohamed for the simulation led to the computation of 2500 grid points in the subdomain of four vortices of Taylor's vortex array. The numbers of grid points used in the x- and z-directions are 50×50 respectively. This mesh size, the automatically determined time step (which was always less than 0·05) and the error tolerance selected (which was $\varepsilon = 10^{-4}$) produced required errors of less than $10^{-5}\%$. Hence for all practical purposes the method was expected to produce the exact solution. This was found to be the case.

The second method applied is the two-step ETUDE method developed by Valentine.[22,23] The ETUDE method is an explicit-in-time, upwind differencing estimate. The finite difference grid for this scheme is illustrated in Figure 2. The application of it to equation (1) is illustrated as part of the algorithm described next.

At time $t = 0$ the vorticity field is specified and the corresponding streamfunction is computed by solving equation (2) by successive overrelaxation. Knowing ψ at $t = 0$, the velocity field is computed by second-order central differences. Once the initial condition is fully defined, the following steps are executed at each interval of time until the desired duration of time has been reached.

Step 1

$$\omega^*_{i,j} = \omega^n_{i,j} - \beta_1 \Delta t \left(\frac{u_R \tilde{\omega}_R - u_L \tilde{\omega}_L}{\Delta x} + \frac{w_T \tilde{\omega}_T - w_B \tilde{\omega}_B}{\Delta z} \right)$$
$$+ \beta_1 \Delta t \left(\frac{\omega^n_{i+1,j} + \omega^n_{i-1,j} - 2\omega^n_{i,j}}{(\Delta x)^2} + \frac{\omega^n_{i,j+1} + \omega^n_{i,j-1} - 2\omega^n_{i,j}}{(\Delta z)^2} \right). \tag{10}$$

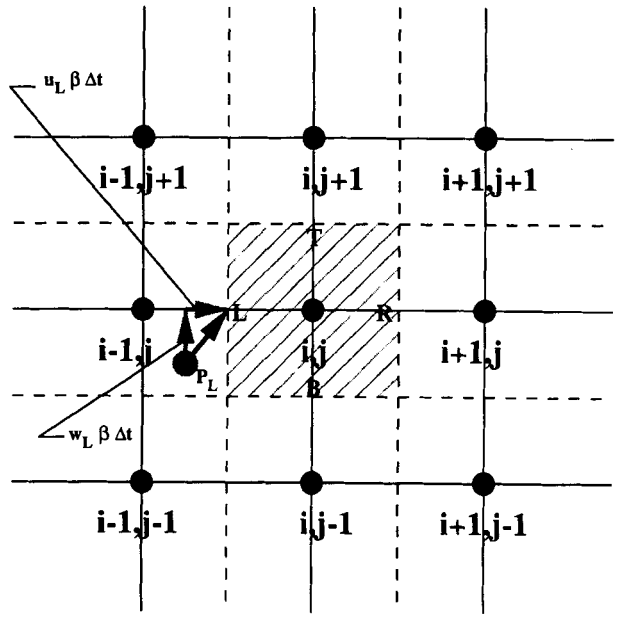

Figure 2. ETUDE scheme finite difference grid

Step 2

$$\psi^*_{i,j} = \left(\frac{\psi^*_{i+1,j} + \psi^*_{i-1,j}}{\Delta x^2} + \frac{\psi^*_{i,j+1} + \psi^*_{i,j-1}}{\Delta z^2} - \omega^*_{i,j}\right)\left(\frac{2}{\Delta x^2} + \frac{2}{\Delta z^2}\right)^{-1}. \tag{11}$$

Step 3

$$u^*_{i,j} = \frac{\psi^*_{i,j+1} - \psi^*_{i,j-1}}{2\Delta z}, \qquad w^*_{i,j} = -\frac{\psi^*_{i+1,j} - \psi^*_{i-1,j}}{2\Delta x}. \tag{12}$$

Step 4

$$\omega^{n+1}_{i,j} = \omega^n_{i,j} - \Delta t\left(\frac{u^*_R\tilde{\omega}_R - u^*_L\tilde{\omega}_L}{\Delta x} + \frac{w^*_T\tilde{\omega}_T - w^*_B\tilde{\omega}_B}{\Delta z}\right) + \Delta t\left(\frac{\omega^*_{i+1,j} + \omega^*_{i-1,j} - 2\omega^*_{i,j}}{(\Delta x)^2} + \frac{\omega^*_{i,j+1} + \omega^*_{i,j-1} - 2\omega^*_{i,j}}{(\Delta z)^2}\right). \tag{13}$$

Step 5

$$\psi^{n+1}_{i,j} = \left(\frac{\psi^{n+1}_{i+1,j} + \psi^{n+1}_{i-1,j}}{\Delta x^2} + \frac{\psi^{n+1}_{i,j+1} + \psi^{n+1}_{i,j-1}}{\Delta z^2} - \omega^{n+1}_{i,j}\right)\left(\frac{2}{\Delta x^2} + \frac{2}{\Delta z^2}\right)^{-1}. \tag{14}$$

Step 6

$$u^{n+1}_{i,j} = \frac{\psi^{n+1}_{i,j+1} - \psi^{n+1}_{i,j-1}}{2\Delta z}, \qquad w^{n+1}_{i,j} = -\frac{\psi^{n+1}_{i+1,j} - \psi^{n+1}_{i-1,j}}{2\Delta x}. \tag{15}$$

The asterisks imply values at the intermediate time step $\beta_1 \Delta t$. The velocities at each face are assumed known and constant over the time step; hence suitable averages of $\tilde{\omega}_R$, $\tilde{\omega}_L$, $\tilde{\omega}_T$ and $\tilde{\omega}_B$ are required over the time interval $\beta_1 \Delta t$ for Step 1 and Δt for Step 4. The method applied to determine these averages is illustrated in Figure 2 for the left face L of the finite difference cell. The point identified as $\mathbf{P}_L$ in the figure is the geometric location at which the value of $\tilde{\omega}_L$ is estimated by bilinear interpolation using the known values of ω at the surrounding four grid points. It is assumed that the interpolated value of ω is the average value for all the fluid particles flowing through face L over the time interval $\beta_1 \Delta t$ in Step 1 and Δt in Step 4. The parameter $|\mathbf{u}|$ is the magnitude of the velocity vector in the direction of the arrow in the figure. The length of the arrow for Step 1 is $\beta\beta_1|\mathbf{u}|\Delta t$. For Step 4 it is $\beta|\mathbf{u}|\Delta t$. The velocity vector for Step 1 is $\mathbf{u} = u_L\hat{\mathbf{i}} + w_L\hat{\mathbf{k}}$, in which u_L and w_L are evaluated at time t (or at the nth time step). For Step 4 it is $\mathbf{u} = u_L^*\hat{\mathbf{i}} + w_L^*\hat{\mathbf{k}}$, in which u_L^* and w_L^* are evaluated at time $t + \beta_1 \Delta t$. The $(n+1)$th time step corresponds to the time $t + \Delta t$. In the present study $\beta_1 = \beta = \frac{1}{2}$ was used. With these values of β_1 and β the scheme is formally first-order in time and second-order in space. This scheme is a transportive upwind control volume method that was designed to have zero second-derivative truncation error in equally spaced grids.

The equations in Steps 2 and 5 are solved by successive overrelaxation (SOR). The convergence criterion specified is such that at every point in the computational domain $\Delta\psi < \varepsilon$, where ε is a small number and $\Delta\psi$ is the change in ψ as computed every 21 iterations. The selection of ε depends on the range of ψ expected and the accuracy required.

The finite difference grid is as follows. For M grid points in the x-direction and N grid points in the z-direction the step sizes in x and z respectively are

$$\Delta x = \frac{1}{M-1}, \qquad \Delta z = \frac{1}{N-1},$$

where the domain is assumed to be square. The subscripts (i, j) in equations (10)–(15) identify grid points located at $x = (i-1)\Delta x$ for $i = 1, 2, \ldots, M$ and $z = (j-1)\Delta z$ for $j = 1, 2, \ldots, N$. Hence the computations are done at $M \times N$ grid points.

To evaluate the code that implemented the ETUDE computational method, one of the 'standard' driven cavity test problems, namely a square cavity with $Re = 1000$, was computed. Figure 3 illustrates the computed streamline pattern for the driven cavity problem with $M \times N = 81 \times 81$. This pattern is equivalent to the streamline pattern reported by Sivaloganathan and Shaw.[28] The vertical height of the lower right recirculation region is approximately 0·35; this is consistent with the range of values summarized for this test problem by Guj and Stella.[29] Finally, the extremum of the streamfunction of the primary vortex is $-0{\cdot}114$, that of the bottom right vortex is $2{\cdot}0 \times 10^{-4}$ and that of the bottom left vortex is $1{\cdot}7 \times 10^{-3}$; these results are the same as the extrema reported by Gresho *et al.*[30] The minimum value of ψ is located at $(x, z) = (0{\cdot}53, 0{\cdot}56)$. A 161×161 grid case was also run; the streamlines and contours of vorticity were equivalent to those for the 81×81 case; the dividing streamlines that separate the core flow from the corner vortices and the contours of zero vorticity were identical for the two cases. The extrema of the streamfunction for the primary, bottom right and bottom left vortices for the 161×161 case are $-0{\cdot}117$, $2{\cdot}0 \times 10^{-4}$ and $1{\cdot}7 \times 10^{-3}$ respectively, which is in reasonable agreement with the 81×81 case. Also, the location of the minimum value of ψ was the same for the two cases. These results compare favourably with the predictions reported by others on this test problem.

Cases 1 and 2 described in the next section were recomputed with the ETUDE scheme to check the computation of temporal evolution. The results from the ETUDE code were found to be in reasonable agreement with the results compared with the fourth-order code. Because the fourth-order code is still under development and the ETUDE scheme code is relatively efficient and uses less computer time, the latter was then used to compute the moderate-$\mathscr{R}$ cases. More specifically, for the 4×4, $\mathscr{R} = 100$

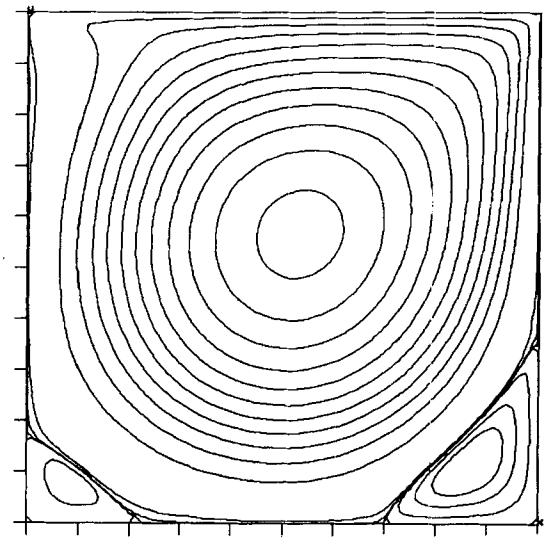

Figure 3. Streamline pattern for driven cavity test problem; $Re = 1000$, 81×81 grid, $-0{\cdot}12 < \psi < 0$ and $\psi = -0{\cdot}0001$, $-0{\cdot}00005$, $-0{\cdot}00001$, $0{\cdot}0001$, $0{\cdot}0005$, $0{\cdot}001$, and $0{\cdot}005$. These are the same streamlines as plotted by Sivaloganathan and Shaw;[28] the comparison is favourable

initial condition case (case 4 in the next section) a 101×101 grid was used. The magnitude of the 2×2 array perturbation was $\mathscr{R}' = 1$. The convergence criterion for the maximum difference in the streamfunction in the SOR routine used to solve equation (2) was $\varepsilon = 0{\cdot}0001$. The non-dimensional time step selected was 10^{-6}. The time interval computed was $0 < t < 0{\cdot}006$. The computations were redone for an 81×81 grid. The results for the two sets of computations were essentially the same.

ETUDE was also used successfully in the two-dimensional study of reservoir charging by Valentine and Yang.[31]. It has more recently been applied successfully to solve the problem of internal solutions approaching a change in bottom topography by Saffarinia.[32] He compared predictions based on ETUDE with experimental data with great success for flows characterized by Reynolds numbers of 1000 and 10,000 based on characteristic wave speed and tank depth. Finally, these examples and the fact that the computation of the square root of the ratio of enstrophy to energy decays monotonically with time for the decaying flow fields reported herein provide evidence that ETUDE is a valid computational method.

3. RESULTS AND DISCUSSION

The global stability theory for Taylor's array was published by Lin and Tobak.[18,19] They showed from energy considerations that this flow field is monotonically and asymptotically stable. They also presented a sufficient condition for energy stability. Chen[20] investigated the linear and non-linear stability of perturbations of the infinite Taylor array of counter-rotating vortices. Even though the flow field decays with time, if it is perturbed, the basic structure of the flow field breaks up or is disarranged. The break-up or disarrangement process depends on the structure or pattern of the disturbances imposed (i.e. the scales inherent in the perturbation). In the present study it is also demonstrated that the disarrangement process depends on the size of the domain (i.e. the lateral confinement) and on the strength of the vortices of the basic state at time $t = 0$.

3.1. *Low-$\mathscr{R}$ cases: linear superposition of modes*

The numerical predictions for three simulations for which $\mathscr{R} = 1$ are described next. These cases are examples of unconditionally stable cases. The effects of the coupling of modes—both the interaction of the mode of the basic state with the modes making up the perturbation and the non-linear interactions between modes—are negligible. However, because large scales decay significantly more slowly than smaller scales, the flow pattern still disarranges. The three cases presented next illustrate this fact.

The initial condition for Case 1 is Taylor's array, namely

$$\omega = -2\pi^2(n^2 + m^2)\mathscr{R} \sin(nx)\sin(mz), \tag{16}$$

where $0 \leq x \leq \pi$, $0 \leq z \leq \pi$, $n = m = 2$, plus an approximately 1% increase in the magnitude of ω at the centre of each positive cell and an approximately 1% decrease in the magnitude of ω at the centre of each negative cell (these are added to the functional representation of the vorticity at the cell centre in the ELLPACK finite element method). This perturbation is like the 'even–even' mode perturbation examined by Chen,[20] which is called the 'odd–odd' mode by Thess.[10] The predicted streamline patterns for $t = 0{\cdot}25$, $0{\cdot}32$, $0{\cdot}48$ and $0{\cdot}89$ are shown in Figures 4–7 respectively. The pairing (or attraction) of vortices of the same sense is observed in Figures 4 and 5. The subsequent merging into a single large-scale structure is observed in Figures 6 and 7. For this case the paired vortices remain stationary along the diagonal of the square domain. This indicates that there are no energy transfers and no linear or non-linear interactions between the basic state and the perturbation. The critical condition for a decaying flow field is the condition such that for a flow that is below critical, energy is *not* transferred from the basic state to the perturbation. Since this is true for Case 1, the solution is dominated by the decay of superimposed Stokes modes (or a linear superposition of Taylor arrays of different sizes). Because this is a linear superposition of two Stokes modes, the non-linear terms computed in the simulation of the solution of equation (1) must cancel. The value of $\mathscr{R} = 1$ is less than the critical value of $3{\cdot}13$; hence Case 1 is expected to be stable.

To illustrate that this solution (which is a direct simulation of the full NS equations) is indeed the linear superposition of Stokes modes, let

$$\psi = \psi^{\mathrm{T}} + \psi',$$

where ψ^{T} is the basic state as calculated from equation (3) and ψ' is what we shall call the perturbation field. Thus

$$\psi' = \psi - \sin(x)\sin(z)e^{-2t},$$

where ψ is the full non-linear solution that was computed numerically.

The perturbation streamfunction ψ' for Case 1 at time $t = 0{\cdot}32$ is illustrated in Figure 8. The perturbation at $t = 0$ for this case is like an array of point vortices of the same strength and sign. This array of vortices merges very rapidly into a single large vortex as illustrated in Figure 8. Hence the flow field in Figure 5 at $t = 0{\cdot}32$ is a linear combination of the basic state and a Taylor array with a cell the same size as the computational subdomain.

To complete our scrutiny of Case 1, let us compare the energy per cell in the 16-cell array having $\mathscr{R} = 1$ at $t = 0$ with the energy per cell of an array with eddies four times larger in spatial dimension but with an amplitude $\mathscr{R}' = 0{\cdot}1$ at $t = 0$. It can be shown that the maximum values of the streamfunction for the two flows are approximately equal at $t = 0{\cdot}3$. At $t = 0{\cdot}32$ the numerically simulated flow field is decomposable into the two arrays just described. Thus for $t > 0{\cdot}3$ the larger eddy is expected to dominate the streamline pattern. Since the long-time solution is a single eddy that started with a magnitude approximately equal to 1% of the magnitude of the smaller eddies, the

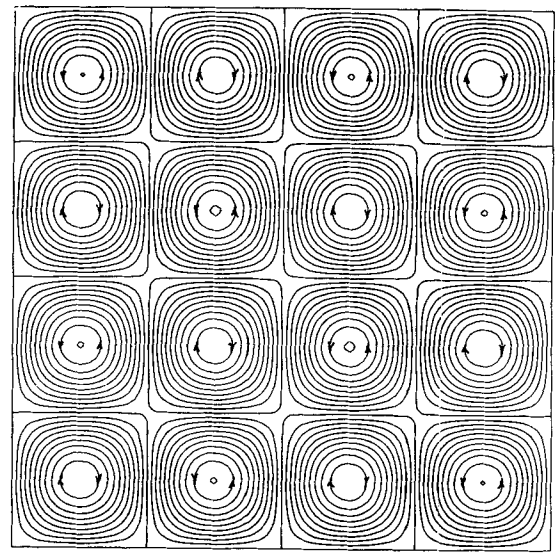

Figure 4. Streamline pattern for Case 1 at $t = 0{\cdot}25$; $-0{\cdot}005 \leq \psi \leq 0{\cdot}013$, $\Delta\psi = 0{\cdot}001$

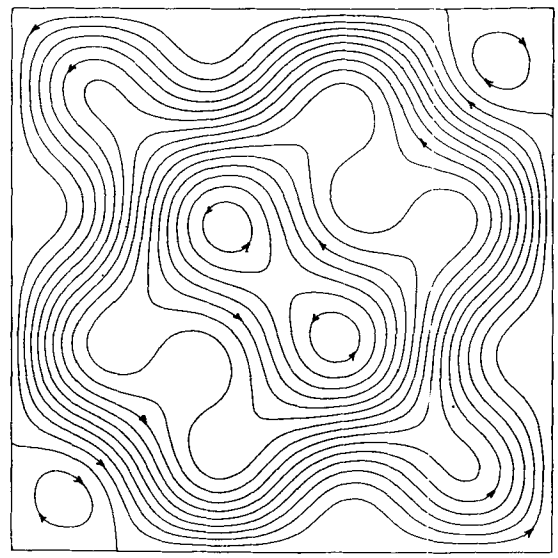

Figure 5. Streamline pattern for Case 1 at $t = 0{\cdot}32$; $-0{\cdot}0005 \leq \psi \leq 0{\cdot}0075$, $\Delta\psi = 0{\cdot}0005$

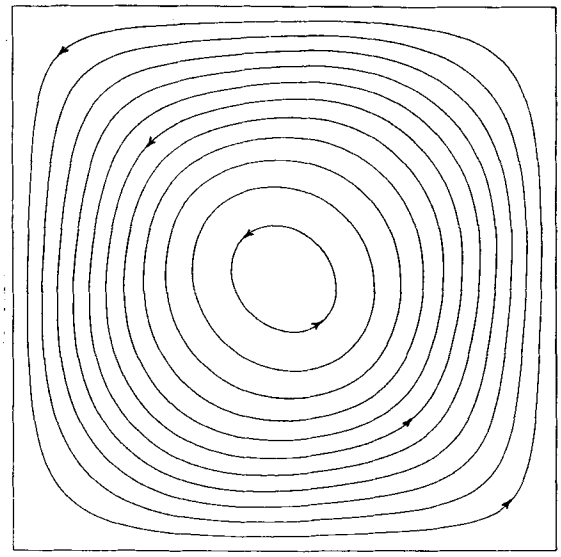

Figure 6. Streamline pattern for Case 1 at $t = 0{\cdot}48$; $0 \leq \psi \leq 0{\cdot}0055$, $\Delta\psi = 0{\cdot}0005$

observed results of the simulation demonstrate that the subcritical disarrangement process for $\mathscr{R} = 1$ is a consequence of the fact that the large-scale structure (or the perturbation) decays significantly more slowly than the smaller-scale structure. Also, since they each decay at a rate independent of each other, there cannot be transfers of energy between the two modes.

The next case considered, Case 2 for $\mathscr{R} = 1$, is the introduction of a perturbation at $t = 0$ that increases the magnitude of ω at the centres of the cells in every other column. It is like the 'odd– even'

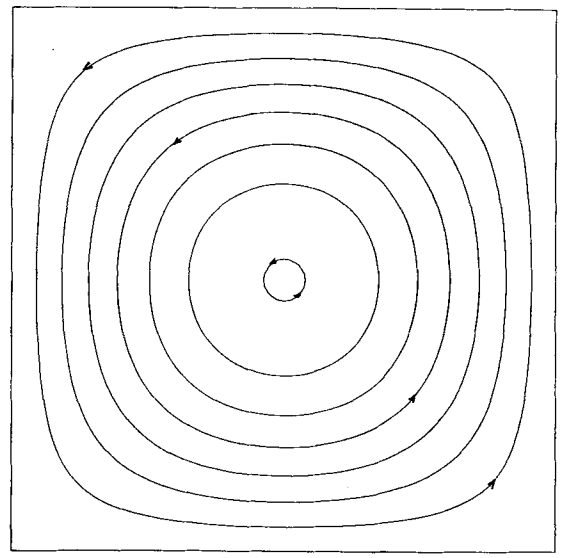

Figure 7. Streamline pattern for Case 1 at $t = 0{\cdot}89$, $0 \leq \psi \leq 0{\cdot}0035$, $\Delta\psi = 0{\cdot}0005$

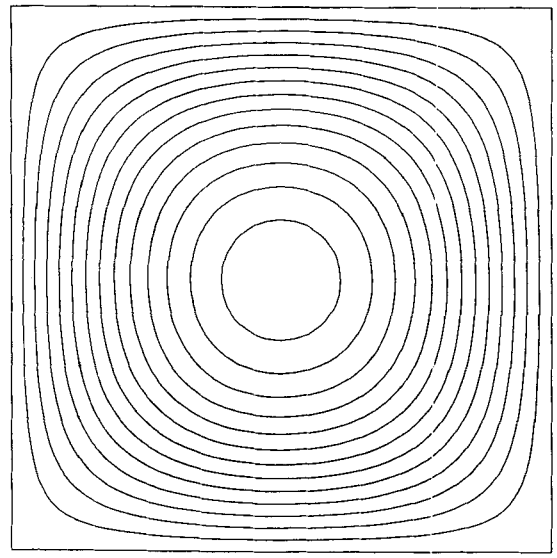

Figure 8. Perturbation streamlines for Case 1 at $t = 0{\cdot}32$; $0 \leq \psi' < 0{\cdot}007$, $\Delta\psi' = 0{\cdot}0005$

mode perturbation examined by Chen.[20] The perturbed columns grow in width while the adjacent columns are compressed. This is illustrated by the predicted evolution of the streamline pattern shown in Figures 9 and 10 for times $t = 0{\cdot}461$ and $0{\cdot}769$ respectively. The perturbed columns grow because the magnitude of the vorticity at their centres was increased by approximately 1%. This perturbation is similar to the 'odd–even' mode perturbation examined by Chen for the infinite domain case. The prediction that the stronger vortices grow in spatial extent while the weaker vortices diminish in size is consistent with the predictions of Chen. The main difference between the present computations and the predictions of Chen is that the symmetry of the flow field is destroyed in the confined domain case. The ultimate structure of the flow field is also different because of the pure slip rigid walls; this is discussed next.

Let us decompose the flow field as we did in the previous case. The structure of the disturbance at $t = 0$ is like two lines of vortex pairs of equal strength a cell width apart. The basic state was subtracted from the solution to extract the disturbance (or perturbation) streamfunction ψ' for the initial condition of Case 2. Contour maps of the perturbation streamfunction ψ' for times $t = 0{\cdot}461$ and $0{\cdot}769$ are shown in Figures 11 and 12 respectively. The like-sign vortices of the disturbance at $t = 0$ merge quickly, forming a double array of elongated vortices. The length scale for the elongated vortices is smaller than the length scale for the largest vortex of Case 1. Hence is it not unexpected that the basic structure of the 4×4 vortex array persists at time $t = 0{\cdot}461$ for Case 2 as compared with the fact that at time $t = 0{\cdot}32$ the array is nearly completely disarranged in Case 1. At $t = 0{\cdot}769$ the lateral growth of the initially stronger vortices is significant. The stronger vortices of like sign would pair and eventually form an elongated set of vortices with a similar structure to the initial disturbance streamfunction at earlier time steps, e.g. at $t = 0{\cdot}461$. This conjecture was verified by computations performed with the ETUDE computational scheme for this case up to $t = 1{\cdot}0$. At $t = 1{\cdot}0$ elongated vortices like the exact solution shown in Figure 13 were predicted. In this figure $\mathscr{R} = 1$, $n = 4\pi$ and $m = \pi$ at $\tau = 0$. The elongated vortices are Taylor modes as well; recall equation (3). Thus in this case, as in Case 1, the disarrangement is due to a superposition of Taylor modes with negligible transfer of energy between modes.

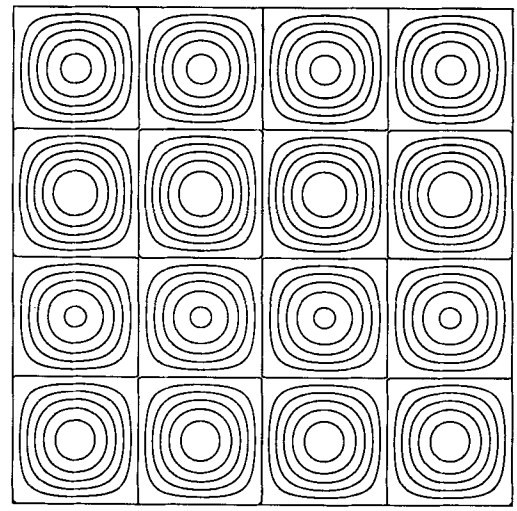

Figure 9. Streamline pattern for Case 2 at $t = 0{\cdot}461$; $-0{\cdot}1 \times 10^{-3} \leq \psi \leq 0{\cdot}1 \times 10^{-3}$, $\Delta\psi = 0{\cdot}2 \times 10^{-4}$

Now let us consider the last $\mathscr{R} = 1$ case, Case 3, in which the magnitude of the vorticity ω at the centres of all 16 vortices is increased. This is like the 'odd–odd' mode perturbation investigated by Chen.[20] In this situation the vortices do not merge. They decay in exactly the same fashion as the original basic state, i.e. the modal structure of the flow field does not break up for this special perturbation. This is because both the perturbation and the basic state have the same modal structure.

3.2. Moderate-$\mathscr{R}$ cases: non-linear modal interactions

The next case we shall examine is Case 4, which demonstrates the *non-linear* break-up of the 4×4 Taylor array with $\mathscr{R} = 100$ when it is perturbed by a 2×2 array with amplitude $\mathscr{R}' = 1$. Note that

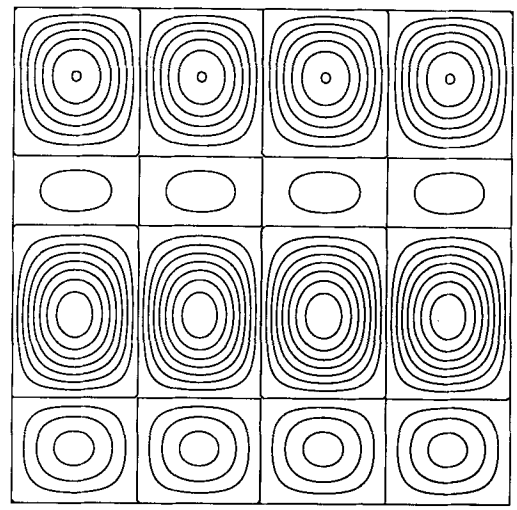

Figure 10. Streamline pattern for Case 2 at $t = 0{\cdot}769$; $-0{\cdot}7 \times 10^{-6} \leq \psi \leq 0{\cdot}7 \times 10^{-6}$, $\Delta\psi = 0{\cdot}1 \times 10^{-6}$

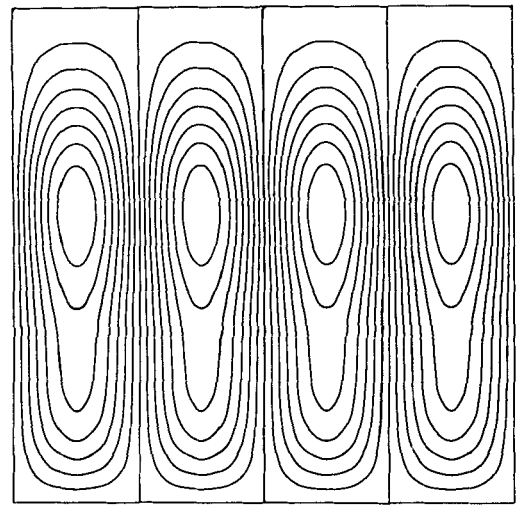

Figure 11. Perturbation streamlines for Case 2 at $t = 0{\cdot}461$; $-0{\cdot}7 \times 10^{-5} \leq \psi' \leq 0{\cdot}7 \times 10^{-5}$, $\Delta\psi' = 0{\cdot}1 \times 10^{-5}$

$\mathscr{R} = 100$ is significantly greater than the critical value of $\mathscr{R}_c = 3{\cdot}13$; hence energy is expected to cascade from the small scale (or basic state) to the large scale (or perturbation field). If we identify each Fourier mode by the number of vortical cell sides in each direction, then from the NS equations the sum of an (n, m)=(4, 4) mode (the basic state) and a (2, 2) mode (the perturbation) interacts to first order through the (6, 2) and (2, 6) modes. Although these modes appear because of the non-linear terms in the NS equations, they are linear interactions in terms of an equation for the perturbation field. The primary non-linear modes that appear in the merging process of like-sign vortices for this case are the (8, 4), (10, 2), (4, 8) and (2, 10) modes. All other modes are negligible or identically zero. (Not all modes are excitable; the only modes that are potentially excitable are the modes that are coupled with

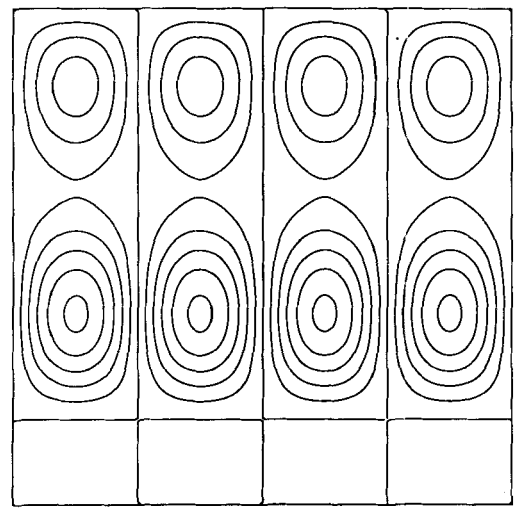

Figure 12. Perturbation streamlines for Case 2 at $t = 0{\cdot}769$; $-0{\cdot}5 \times 10^{-6} \leq \psi' \leq 0{\cdot}5 \times 10^{-6}$, $\Delta\psi' = 0{\cdot}1 \times 10^{-6}$

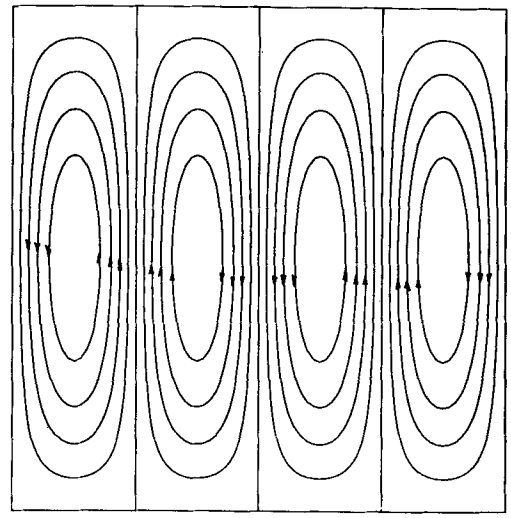

Figure 13. Elongated vortices—another non-parallel flow exact solution

the basic state through the non-linear terms of the NS equations.) The time evolution of the streamline pattern is illustrated in Figures 14(a)–14(c) for $t = 0{\cdot}0002$, $0{\cdot}0015$ and $0{\cdot}006$ respectively. Note that the strong vortices that pair and eventually merge revolve in the direction of the energized 2×2 array. Figure 15 presents the results of the Fourier decomposition for this flow field. The energy in this case is indeed transferred from the basic state to the perturbation. From $0 < t < 0{\cdot}001$, where $t = m^{-2}t$ and m is the mode number or number of vortex cells in each direction of the basic state, the flow field decays at the exponential decay rate associated with the 4×4 Taylor array. Over the range $0{\cdot}001 < t < 0{\cdot}006$ a transition occurs during which like-sign vortices merge. The merging process involves a rapid increase in the energy of the perturbation at the expense of a rapid decrease in energy from the basic state at the onset of transition (or merging). Then there is an oscillatory adjustment in energy between the modes until the flow field settles down at $t = 0{\cdot}006$, at which time the flow field has the structure of the 2×2 array. The decay rate for $t > 0{\cdot}006$ is essentially the same as the decay rate for a 2×2 Taylor array.

The largest scale of motion that was imposed on the system at $t = 0$ was the 2×2 array. It is this scale that dominates the final decay process of the perturbed Taylor flow. Hence the final structure of the flow field that persists at a long time from the initial condition is the largest scale imposed initially on the system. This is also true because the perturbation imposed is an even–even mode. The modal interaction between the 4×4 basic state and the 2×2 perturbation has no link to scales larger than 2×2. The sums and differences of the mode numbers are the only modes energized by the non-linearities in the NS equation; thus only modes related to even integers of mode number are energized in this case. Hence no global rotation arises and no structures larger than 2×2 arise in the ultimate state of this case. The size of the subdomain is important only to the extent that it represents the largest possible scale that may be imposed in a particular numerical simulation. Since the largest scale contained in the perturbation of this example is less than the largest scale of the domain (i.e. the distance between the walls of the domain), the largest scale in the perturbation dominates the long-time decay process. Hence the flow remembers its initial condition.

The next case, Case 5, is the disarrangement of a 2×2 Taylor array with an initial amplitude of $\mathscr{R} = -50$ caused by a perturbation with an initial structure of a 3×3 array with an amplitude of

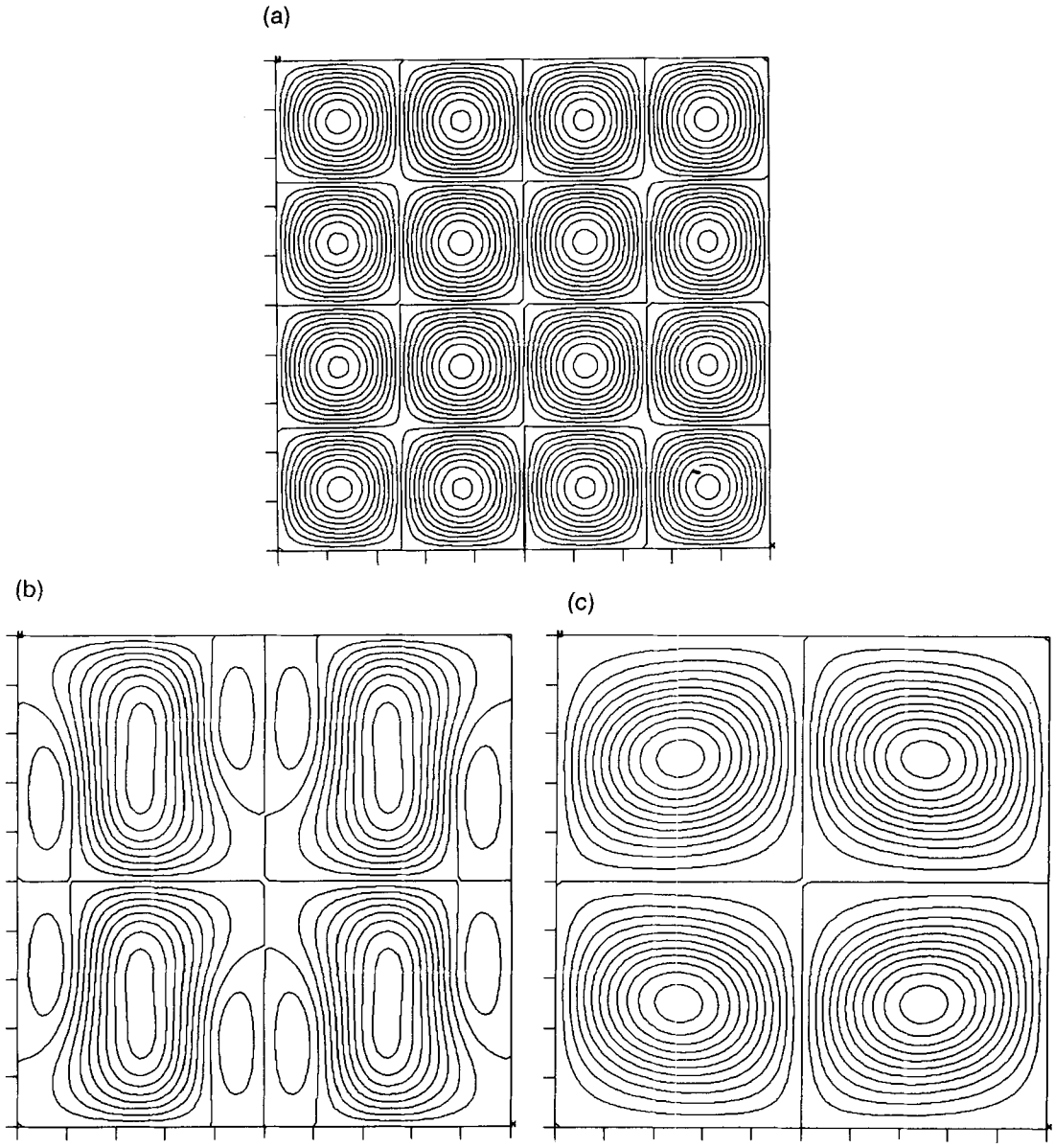

Figure 14. Case 4: non-linear break-up of 4 × 4 array with $\mathscr{R} = 100$ perturbed at $t = 0$ by 2 × 2 array with $\mathscr{R}' = 1$. Streamline patterns: (a) $t = 0{\cdot}0002$, $-100 < \psi < 100$, $\Delta\psi = 10$; (b) $t = 0{\cdot}0015$, $-80 < \psi < 80$, $\Delta\psi = 10$; (c) $t = 0{\cdot}006$, $-60 < \psi < 60$, $\Delta\psi = 5$

$\mathscr{R}' = 1{\cdot}0$. The streamline pattern at $t = 0{\cdot}010$ is shown in Figure 16. If the mode corresponding to the basic state, i.e. the (2, 2) mode, is subtracted from the flow field, the perturbation that is left at $t = 0{\cdot}010$ is as illustrated in Figure 17(a). The corresponding perturbation vorticity is shown in Figure 17(b). Figures 17(a) and 17(b) look exactly like the 'first unstable mode' for the driven lattice; compare with Figures 4(b) and 4(a) respectively in Reference 10. (Note that the plots in Figure 4 of Thess's paper must be relabelled to be correct, i.e. 4(a) is actually 4(b) and vice versa. A preprint had it

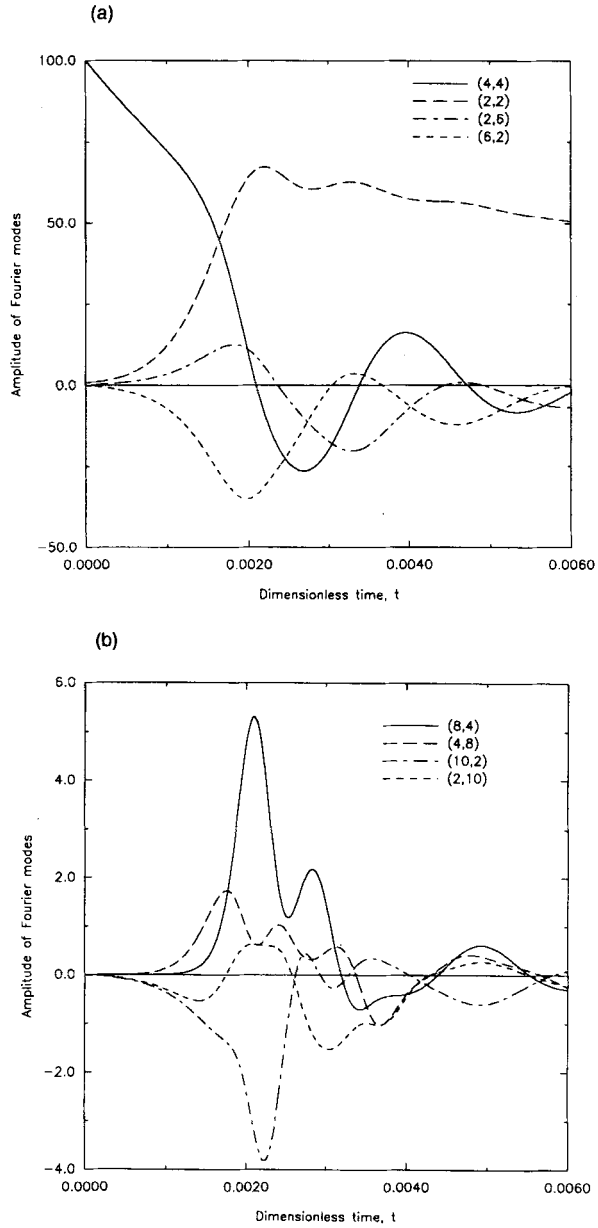

Figure 15. Evolution of Fourier modes that illustrate break-up of Case 4 vortical array: (a) (4, 4) basic state, (2, 2) perturbation and linearly excited Fourier modes; (b) principal non-linearly excited modes

correct.) The onset of merging of the two dominant vortices may be observed in Figure 16. Subsequent to the merging (or capture) event the flow field approaches a flow pattern with a single-cell structure. The streamlines and vorticity contours for $t = 0{\cdot}045$ are presented in Figure 18. This is an instant of time at the end of the merging event. The principal Fourier modes for this case are presented in Figure 19. The square roots of the ratios of palinstrophy to enstrophy and enstrophy to energy are plotted as

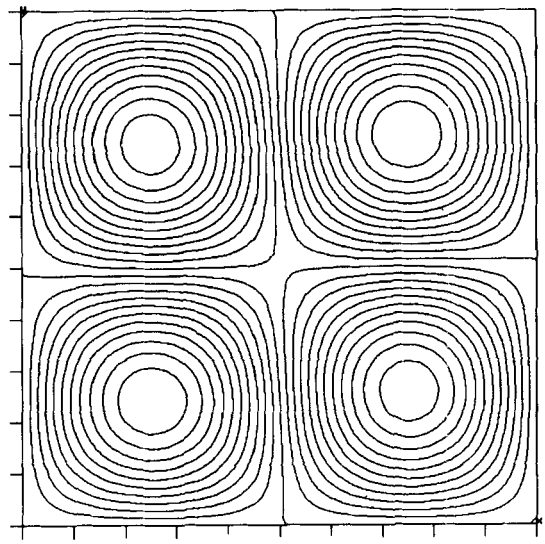

Figure 16. Case 5: streamline pattern at $t = 0{\cdot}010$, $-22 < \psi < 24$, $\Delta\psi = 2$ illustrating initiation of non-linear break-up of 2×2 array with $\mathscr{R} = -50$ perturbed at $t = 0$ by 3×3 array with $\mathscr{R}' = 1$

functions of time in Figures 20 and 21 respectively. The merging event is characterized by a peak in the $\sqrt{(P/\Omega)}$ curve. The $\sqrt{(\Omega/E)}$ curve decays monotonically with time as it should.

Let us next examine the modal interactions that occur and that lead to the enhancement of global rotation of the confined vortex lattice of Case 5. The (3, 3) perturbation interacts with the (2, 2) basic state initially through the (5, 1) and (1, 5) modes. The structure of the most unstable mode in the

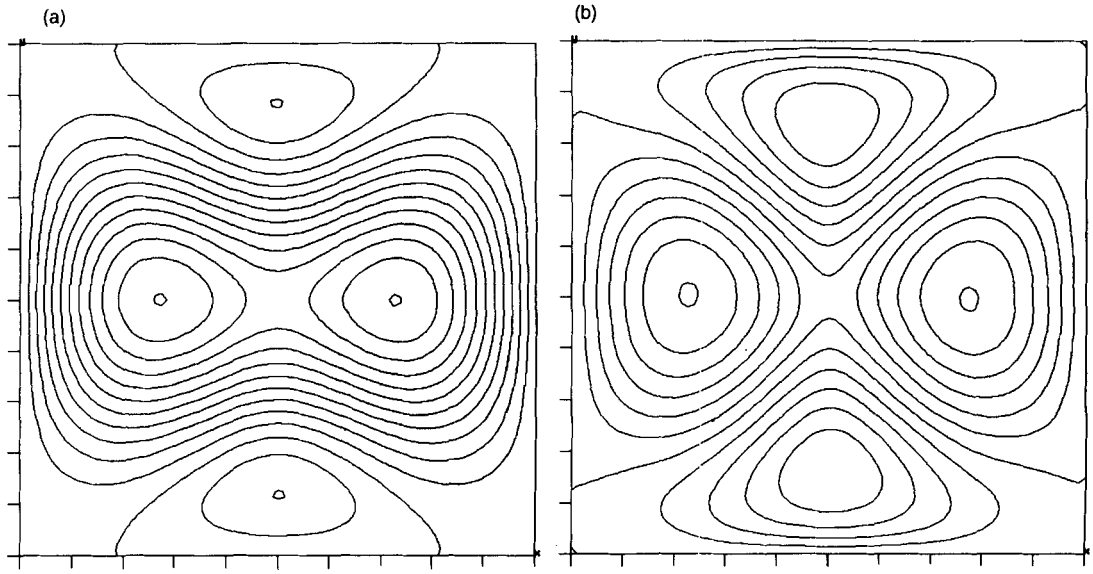

Figure 17. Case 5—structure of perturbation at $t = 0{\cdot}010$: (a) perturbation streamlines, $-0{\cdot}6 < \psi' < 2{\cdot}4$, $\Delta\psi' = 0{\cdot}2$; (b) perturbation vorticity, $-140 < \omega' < 100$, $\Delta\omega' = 20$

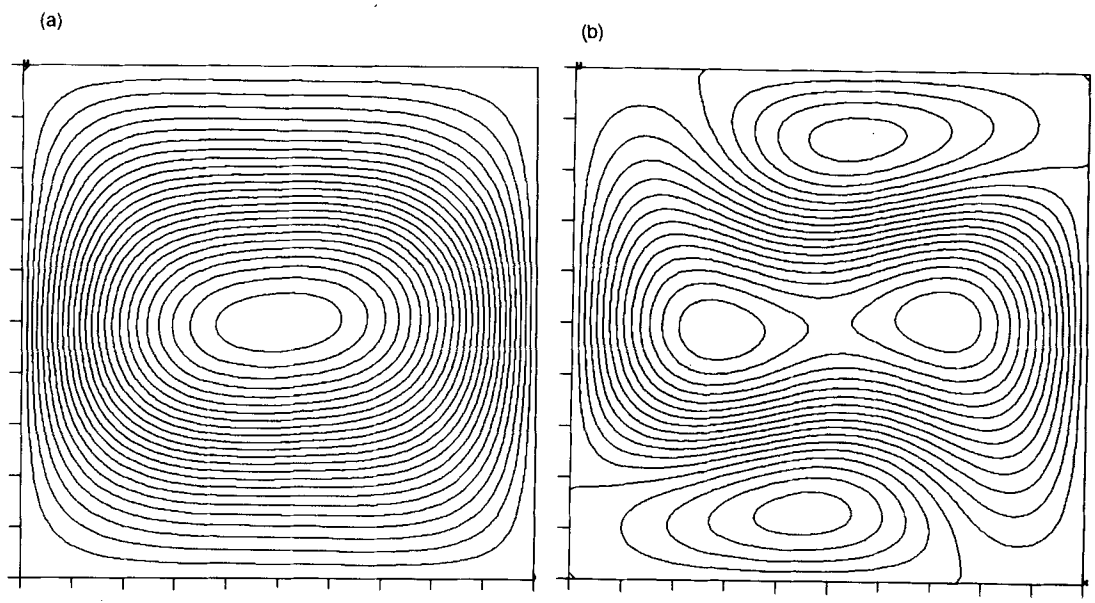

Figure 18. Case 5: (a) streamline pattern at $t = 0{\cdot}045$, $-0{\cdot}2 < \psi < 5$, $\Delta\psi = 0{\cdot}2$; (b) vorticity contours, $-140 < \omega < 50$, $\Delta\omega = 10$

perturbation of the 2 × 2 basic lattice is made up primarily of a linear combination of (3, 1), (1, 3) and (1, 1). Thus, subsequently, (5, 1) and (1, 5) interact with the basic (2, 2) mode to induce growth of (3, 1) and (1, 3). The latter two interact with (2, 2) to induce growth of the (1, 1) mode, which is the mode that characterizes the enhancement of global rotation within the flow domain. If the perturbation did not contain an odd-numbered mode, then the (1, 1) mode could not be excited. This fact was

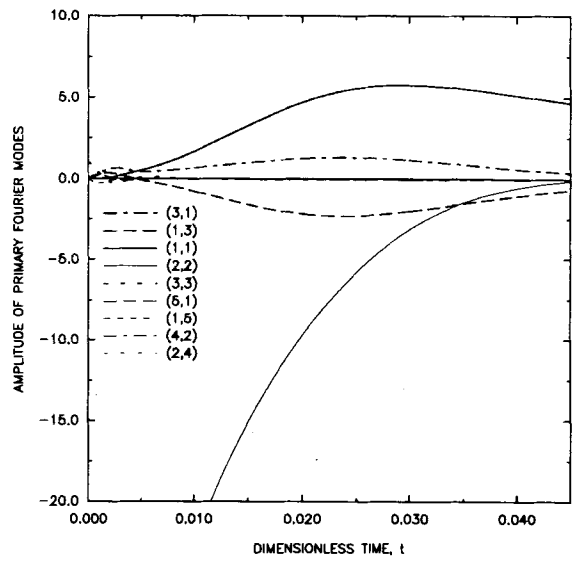

Figure 19. Evolution of principal Fourier modes of Case 5: (2, 2) basic state, (3, 3) perturbation, linearly excited modes and non-linearly excited modes

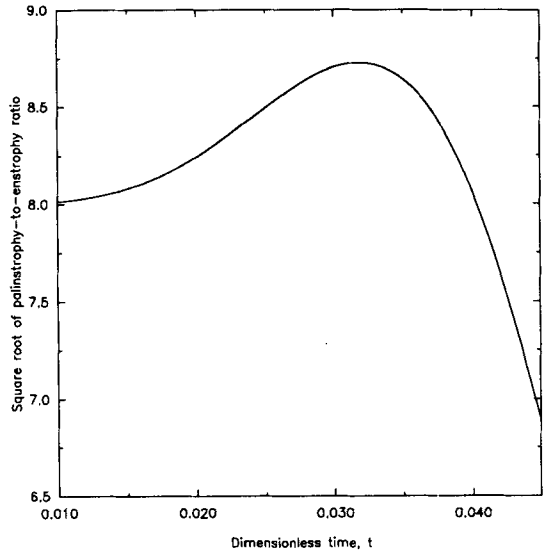

Figure 20. Case 5: square root of palinstrophy/enstrophy ratio versus t for 2×2 array with $\mathscr{R} = -50$ perturbed at $t = 0$ by 3×3 array with $\mathscr{R}' = 1$

demonstrated in the Case 4 simulation. Interestingly, however, the merging (or capture) event simulated in Case 5 occurs in each quadrant of the Case 4 numerical experiment because of the 'conservation' of modes discussed here. In other words, only a portion of the modes in Fourier space are excitable through the coupling (or paths) provided by the non-linear terms in equation (1). Thus the modes excited depend on the modes that exist in the initial condition.

The dominant modes at $t = 0{\cdot}045$ for Case 5 are illustrated in Figure 19. The basic state mode, i.e.

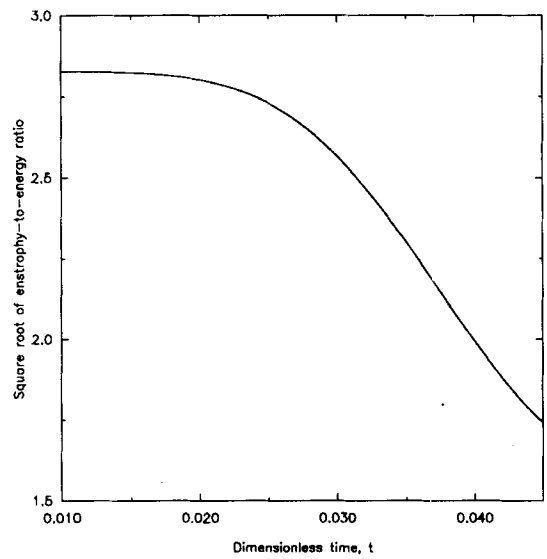

Figure 21. Case 5: square root of enstrophy/energy ratio versus t for 2×2 array with $\mathscr{R} = -50$ perturbed at $t = 0$ by 3×3 with $\mathscr{R}' = 1$

the (2, 2) mode, is small in comparison with the 'most unstable mode', which is the sum of (1, 3), (3, 1) and (1, 1). Note that (4, 2) and (2, 4) are the next largest modes, followed by (5, 1) and (1, 5). The three dominant modes at this time step are (3, 1), (1, 3) and (1, 1). It is an interesting fact that the most persistent mode is the combination of modes that are primary constituents of the 'most unstable mode' (or 'first unstable mode') reported by Thess for the driven lattice case and also predicted by the stability theory described in the previous section. The merging of the vortices of like sense is driven by this modal combination; hence the linear theory does provide some insight to the vortex-merging event. It shows that it is a result of the growth of a linearly unstable mode.

A series of cases were executed over a range of $\mathscr{R}$ to determine, at least approximately, the critical value of this parameter for the 2×2 basic state. The perturbation applied was a 3×3 array with an amplitude that is 1% of the value of $\mathscr{R}$ for the basic state. The critical value predicted is $\mathscr{R}_c \approx 3{\cdot}5$. This is significantly larger than the energy stability bound derived by Lin and Tobak,[18] namely $\mathscr{R}_{ce} = 2/\pi^2 \approx 0{\cdot}2$. It is less than the linear stability value, namely $\mathscr{R}_{cL} \approx 4{\cdot}2$. The fact that the actual critical value is greater than the sufficient condition for energy stability and less than the necessary condition for linear instability is expected.

For the infinite array of Taylor vortices, Chen[20] predicted the critical condition for non-linear stability as $\mathscr{R}_c = 1{\cdot}05$. The energy stability criterion reported by Lin and Tobak[18] gives a sufficient condition of zero for an infinite array. The linear theory gives for this case a critical value of $\mathscr{R}_{cL} \approx 2{\cdot}8$. Hence, as expected, the actual critical value is between the two bounds.

4. CONCLUSIONS

The onset of the break-up or disarrangement of Taylor's vortex array when an appropriately selected perturbation is imposed was simulated. The pairing and subsequent merging of vortices of like sense were predicted. These results are consistent with recent theoretical results that have been reported by Lin and Tobak[18] and Chen.[20] For $\mathscr{R} = 100$, which is significantly larger than the critical value of $\mathscr{R}$, vortex merging in a confined region of 4×4 vortical cells when perturbed by a 2×2 mode with a unit amplitude was predicted. The energy increases at the scale representative of the emerging vortex, i.e. energy is transferred from mode (4, 4) to mode (2, 2) through the smaller-scale modes, primarily (6, 2) and (2, 6) and subsequently (4, 8), (10, 2), (4, 8) and (2, 10).

The apparent break-up process for the $\mathscr{R} = 1$ cases is dominated by a linear superposition of Taylor modes that decay independently with time. This value of $\mathscr{R}$ is less than the critical; hence the non-linearities are negligible and there is negligible energy transfer between all the modes in the initial condition. This is in contrast with the $\mathscr{R} = 100$ cases, for which vortex merging occurs with a dramatic transfer of energy from the the basic state to the perturbation. The paired vortices in the latter case rotate in the direction of the larger-scale vortices in which they merge. Thus for large $\mathscr{R}$ the energy in the perturbation increases by extracting energy from the basic state. It subsequently decays. Of course, the total energy decays monotonically with time.

The critical value of the lattice Reynolds number $\mathscr{R}$ was predicted for the 2×2 lattice and compared with the sufficient condition for unconditional (energy) stability and the necessary condition for instability estimated by linear stability considerations. If $\mathscr{R}$ is greater than critical, energy is transferred from the basic state to the perturbation. The lower bound for this parameter based on energy stability arguments is 0·2. The upper bound for this parameter based on linear stability is approximately 4·2. The numerically determined critical value is $\mathscr{R}_c \approx 3{\cdot}5$; it is between the bounds as expected. For the infinite lattice the upper bound is approximately 2·8. Chen[20] found the actual critical value to be $\mathscr{R} = 1{\cdot}05$. Thus lateral confinement enhances stability.

If a decaying vortex lattice contains more than one Taylor mode at time $t = 0$, then the flow pattern will always disarrange, with the largest scale dominating the long-time behaviour of the flow field. The

pairing and merging process is sensitive to the initial conditions imposed. Part of the disarrangement and decay process can be explained by the well-known fact that large scales decay more slowly than smaller scales. If odd modes are present in the initial condition, global rotation of the flow in a confined system will be enhanced if the value of $\mathscr{R}$ is greater than critical. If $\mathscr{R}$ is greater than critical, some energy is transferred from smaller scales to larger scales (the inverse cascade). The stronger vortices, i.e. the vortices perturbed in a manner that increases their strength, tend to dominate the weaker vortices. The pairing and subsequent merging (or capture) of vortices of like sense into larger-scale vortices are characterized by peaks in the evolution of the square root of the palinstrophy divided by the enstrophy.

REFERENCES

1. J. C. McWilliams, 'A demonstration of the suppression of turbulent cascade by coherent vortices in two-dimensional turbulence', *Phys. Fluids A*, **2**, 547 (1990).
2. W. H. Matthaeus, W. T. Stribling, D. Martinez, S. Oughton and D. Montgomery, 'Decaying, two-dimensional, Navier–Stokes turbulence at very long time', *Physica D*, **51**, 531–538 (1991).
3. G. I. Taylor, 'On the decay of vortices in a viscous fluid', *Philos. Mag.*, **46**, 671–674 (1923).
4. J. S. A. Green, 'Two-dimensional turbulence near the viscous limit', *J. Fluid Mech.*, **62**, 273–287 (1974).
5. K. Gotoh, M. Yamada and J. Mizushima, 'The theory of stability of spatially periodic flows', *J. Fluid Mech.*, **127**, 45–58 (1983).
6. K. Gotoh and M. Yamada, 'Instability of a cellular flow', *J. Phys. Soc. Jpn.*, **53**, 3395–3398 (1984).
7. D. N. Beaumont, 'The stability of spatially periodic flows', *J. Fluid Mech.*, **108**, 461–474 (1981).
8. U. Frish and P. L. Sulem, 'Numerical simulation of the inverse cascade in two-dimensional turbulence', *Phys. Fluids*, **27**, 1921–1923 (1984).
9. A. Thess, 'Instabilities in two-dimensional spatially periodic flows. Part I: Kolmogorov flow', *Phys. Fluids A*, **4**, 1385–1395 (1992).
10. A. Thess, 'Instabilities in two-dimensional spatially periodic flows. Part II: Square eddy lattice', *Phys. Fluids A*, **4**, 1396–1407 (1992).
11. J. Sommeria, 'Experimental study of the two-dimensional inverse energy cascade in a square box', *J. Fluid Mech.*, **170**, 139–168 (1986).
12. J. Sommeria and J. Verron, 'An investigation of nonlinear interactions in a two-dimensional recirculating flow', *Phys. Fluids*, **27**, 1918–1923 (1984).
13. J. Verron and J. Sommeria, 'Numerical simulation of a two- dimensional turbulence experiment in magnetohydrodynamics', *Phys. Fluids*, **30**, 732–739 (1987).
14. N. Platt, L. Sirovich and N. Fitzmaurice, 'An investigation of chaotic Kolmogorov flows', *Phys. Fluids A*, **3**, 681–696 (1991).
15. C. Eringen, *Mechanics of Continua*, Wiley, New York, 1967.
16. L. Rosenhead (ed.), *Laminar Boundary Layers*, Dover, New York, 1966.
17. L. S. G. Kovasznay, 'Laminar flow behind a two-dimensional grid', *Proc. R. Soc.*, **44**, 58–62 (1948).
18. S. P. Lin and M. Tobak, 'Spectral stability of Taylor's vortex array', *Phys. Fluids*, **29**, 3477–3478 (1986).
19. S. P. Lin and M. Tobak, 'Nonlinear stability of Taylor's vortex array', *Phys. Fluids*, **30**, 605–606 (1987).
20. H. B. Chen, 'Instability of nonparallel flows', *Ph.D. Thesis*, Clarkson University, Potsdam, NY, 1989.
21. A. G. Mohamed, D. T. Valentine and R. E. Hassel, 'Numerical study of laminar separation over an annular backstep', *Comput. Fluids*, **20**, 121–143 (1991).
22. D. T. Valentine, 'Comparison of finite difference methods to predict passive contaminant transport', *ASME Computers in Engineering 1987*, Vol. 3, ASME, New York, 1987, pp. 263–269.
23. D. T. Valentine, 'Control-volume finite difference schemes to solve convection diffusion problems', *ASME Computers in Engineering 1988*, Vol. 3, ASME, New York, 1988, pp. 111–117.
24. J. R. Rice and R. F. Boisvert, *Solving Elliptic Problems Using ELLPACK*, Springer, New York, 1985.
25. J. J. Dongarra, J. R. Bunch, C. B. Moler and G. N. Stewart, *LINPACK Users' Guide*, SIAM, Philadelphia, PA, 1979.
26. D. T. Valentine and A. G. Mohamed, 'Higher-order Navier–Stokes solver and a new test problem', *Bull. Am. Phys. Soc.*, **33**, 2265 (1988).
27. D. T. Valentine and A. G. Mohamed, 'Taylor's vortex array: a new test problem for Navier–Stokes solution procedures', in J. Kane and A. Carlson (eds), *Solution of Superlarge Problems in Computational Mechanics*, Plenum, New York, 1989, pp. 167–181.
28. S. Sivaloganathan and G. L. Shaw, 'A multigrid method for recirculating flows', *Int. j. numer. methods fluids*, **8**, 417–440 (1988).
29. G. Guj and F. Stella, 'Numerical solutions of high- *Re* recirculating flows in vorticity–velocity form', *Int. j. numer. methods fluids*, **8**, 405–416 (1988).

30. P. M. Gresho, S. T. Chan, R. L. Lee and C. D. Upson, 'A modified finite element method for solving the time-dependent, incompressible Navier–Stokes equations. Part 2: Applications', *Int. j. numer. methods fluids*, **4**, 619–640 (1984).
31. D. T. Valentine and G. Yang, 'Buoyancy-driven flows in two-dimensional reservoirs: a numerical investigation', *Proc. 1st NFDC*, Vol. 3, 1988, pp. 2036–2043.
32. K. Saffarinia, 'Numerical and experimental study of the interaction of an internal solitary wave with a slope-shelf topography', *Ph.D. Dissertation*, The Catholic University of America, Washington, DC, 1991.